

Fig. 2. $\text{Cd}_{1-x}\text{Mn}_x\text{S}$, $x = 0.0625$ supercell: a – bulk configuration; b – density of states

The electron band structure of $\text{Cd}_{1-x}\text{Mn}_x\text{S}$ ($x = 0.0625$) SMSC is determined from the projected density of states (PDOS) (Fig. 3). The obtained PDOS plots are presented in Fig. 3. The analysis of these graphs shows that in the valence band, the electron band structure of $\text{Cd}_{1-x}\text{Mn}_x\text{S}$ consists of three parts: (1) the upper part of the valence band is mainly formed by p -orbitals of S and Cd atoms, s -orbitals of Cd and Mn atoms with some contribution of d -orbitals of Mn atoms; (2) the middle part is formed by d -orbitals of Cd atoms, which are 8–9 eV lower than the valence band maximum (3) the lower part is formed by s -orbitals of S and Mn atoms, and p -orbitals of Mn atoms which are located 13 eV lower than the valence band maxim. The bottom of the conductivity band is formed by s - and p -orbitals of Mn atoms and p -orbitals of Cd atoms, d -orbitals of S atoms (Fig. 3).

The band gap for the $\text{Cd}_{1-x}\text{Mn}_x\text{S}$ SMSC with $x = 0.25$ supercells is equal to $E_g = 1.6$ eV and total energy is equal to $E_t = -6698.61546$ eV. For the $x = 0.0625$ supercell band gap is equal to $E_g = 1.25$ eV and total energy is equal to $E_t = 59267.92943$ eV. The calculated band gap much closer to theoretical 1.25 eV, 1.27 eV [12,20] and experimental value [26]. The values of band gap with GGA calculations and effect of Hubbard "U" term on band gap using GGA+U calculations were used in [12,20].

Calculations show that the band gap increase with an increase in Mn ion concentration (Table 1). These theoretical results have a good agreement with experimental results [27]. The optical transmission of the $\text{Cd}_{1-x}\text{Mn}_x\text{S}$ thin films show that the band gap increases with the increases in manganese ion concentration.

Table 1. Band gap and total energy for $\text{Cd}_{1-x}\text{Mn}_x\text{S}$

x	E_g , eV	E_t , eV
0	0.83	-1910,95
0.0625	1.25	-59267,93
0.25	1.6	-6698,62

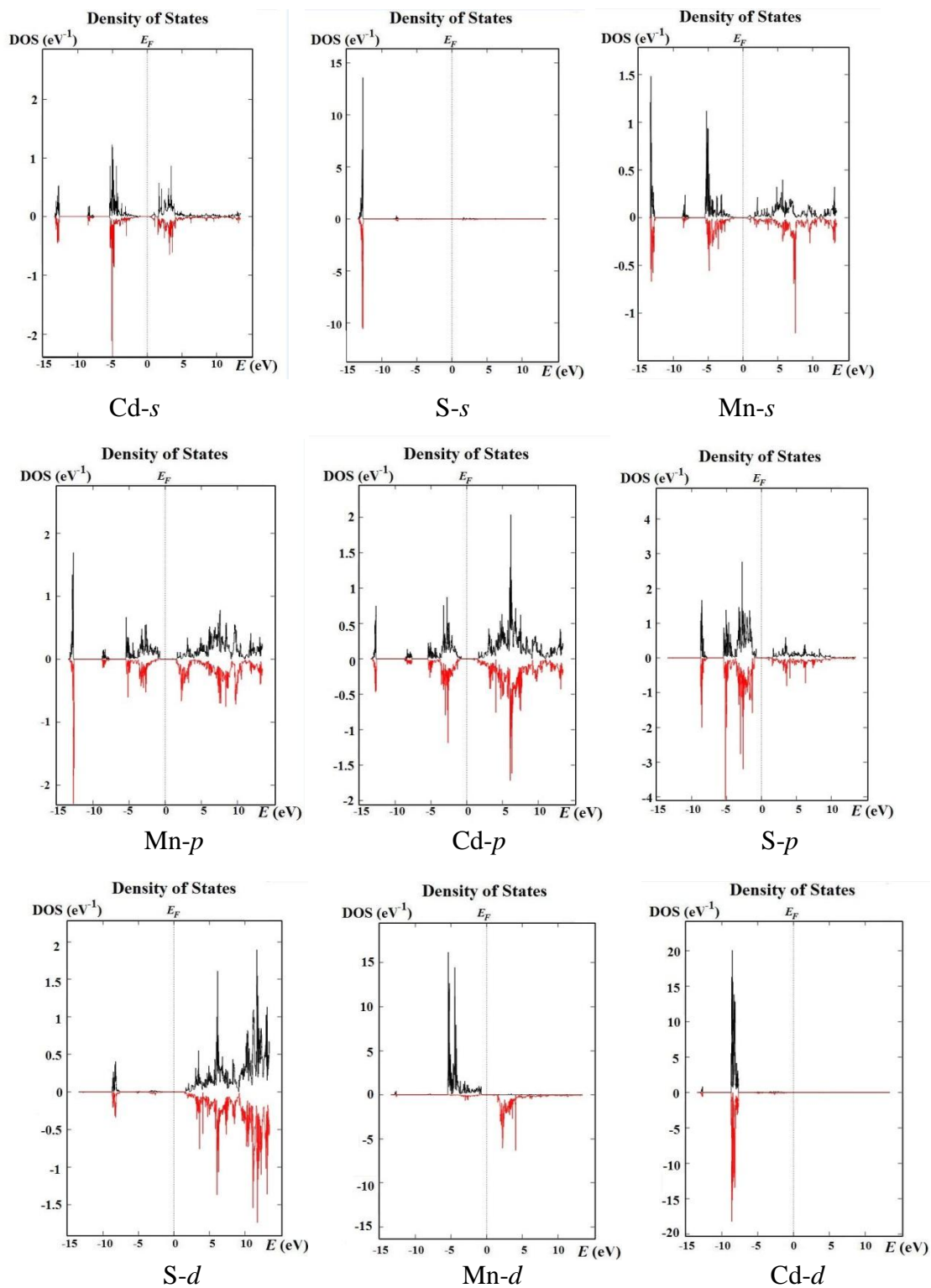


Fig. 3. PDOS of $\text{Cd}_{1-x}\text{Mn}_x\text{S}$ ($x = 0.0625$) SMSC

EBS and DOS of the defective $\text{Cd}_{30}\text{Mn}_2\text{Se}_{32}$ supercell are calculated. We consider vacancy-type defects. Atom relaxation and optimization of the crystal structure were carried out, and forces and stresses were minimized (Fig. 4).

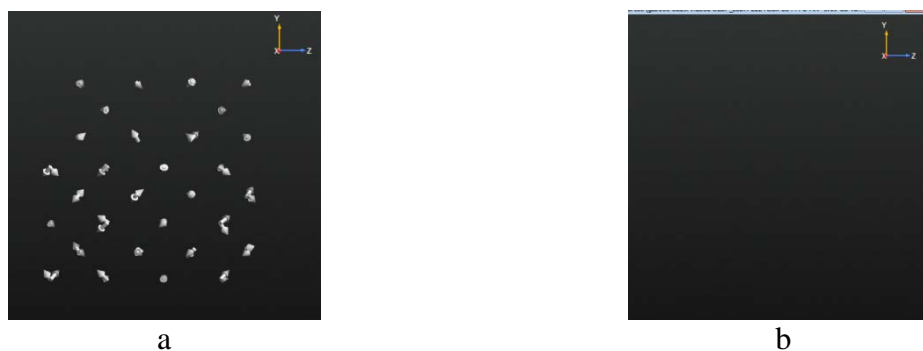


Fig. 4. Forces: a – before optimization; b – after optimization

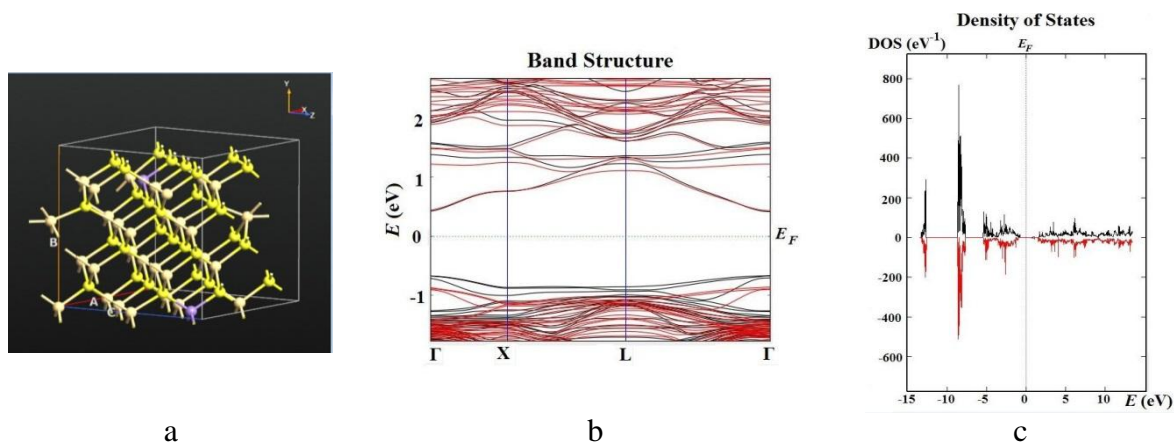


Fig. 5. S vacancy in $Cd_{1-x}Mn_xS$, $x = 0.625$; a – bulk configuration; b – EBS; c – DOS

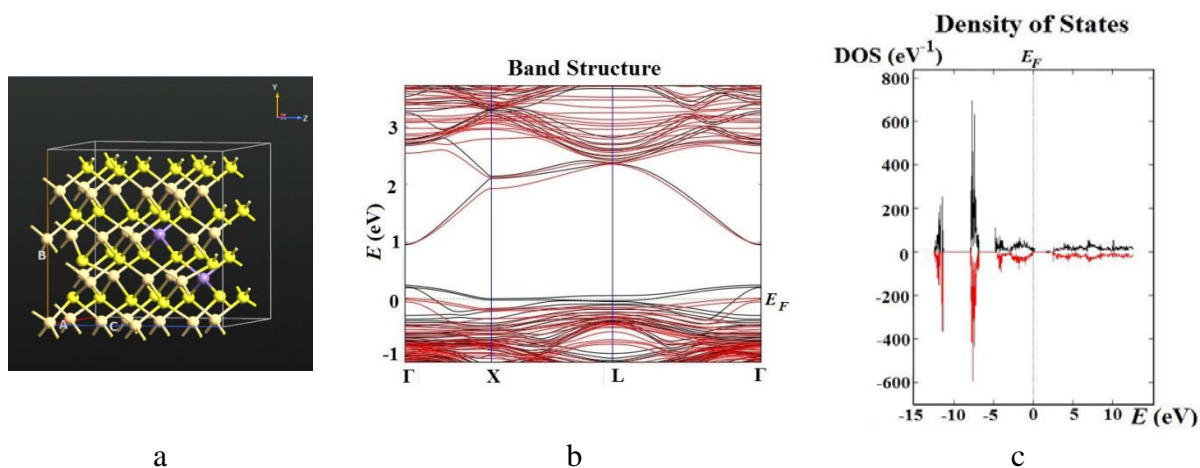


Fig. 6. Cd vacancy in $Cd_{1-x}Mn_xS$, $x = 0.625$; a – bulk configuration; b – EBS; c – DOS

In the case of S vacancy (V_S), the band gap is $E_g = 1.3$ eV, and the total energy equals $E_t = -58907.65$ eV (Fig. 5); for Cd vacancy (V_{Cd}) the band gap is $E_g = 1.55$ eV, the total energy is $E_t = -57712.51$ eV (Fig. 6). Figures 5 and 6 show that Cd or S vacancy in a crystal leads to an increase in the band gap, as a change in the total energy occurs, the Fermi level shifts towards the valence or conduction band.

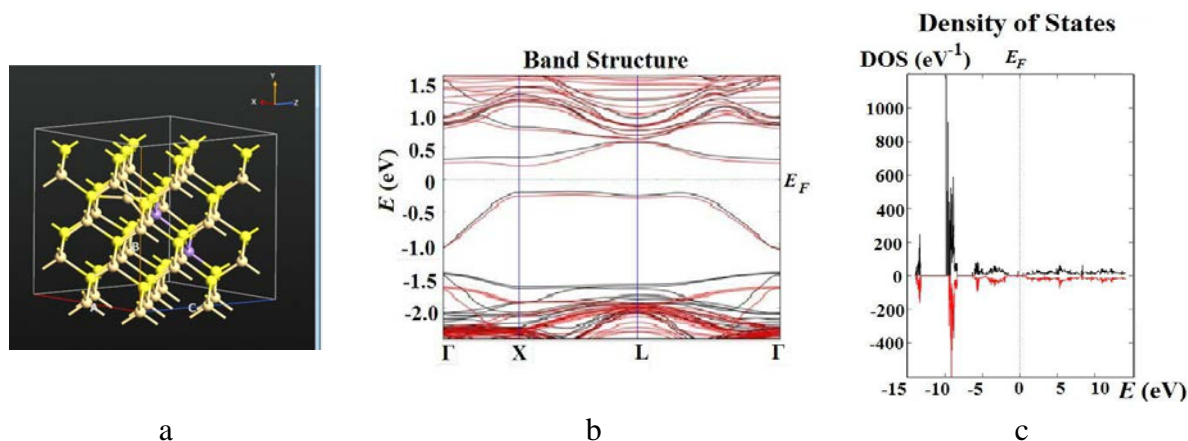


Fig. 7. Interstitial Cd atom in $\text{Cd}_{1-x}\text{Mn}_x\text{S}$, $x = 0.625$; a – bulk configuration; b – EBS; c – DOS

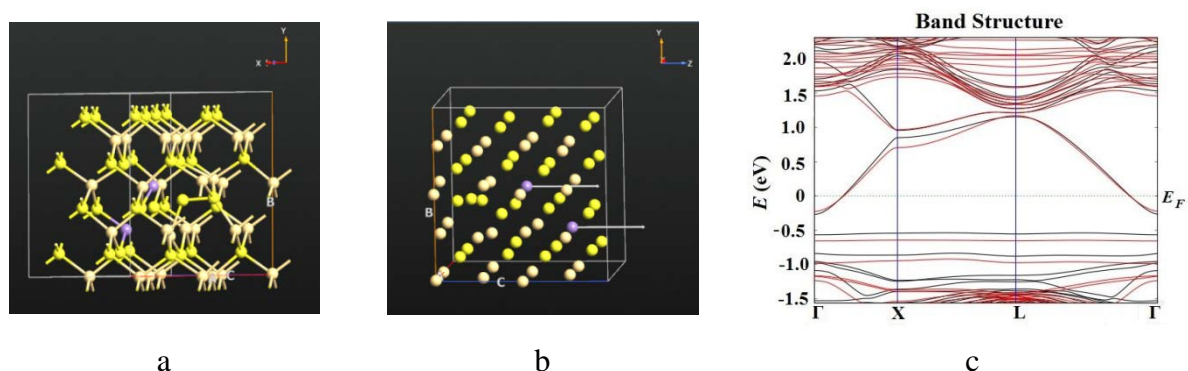


Fig. 8. Interstitial S atom in $\text{Cd}_{1-x}\text{Mn}_x\text{S}$, $x = 0.625$; a – bulk configuration; b – magnetic moments; c – EBS

Supercell of $\text{Cd}_{1-x}\text{Mn}_x\text{S}$ of 64 atoms with interstitial Cd (I_{Cd}) atom and interstitial S (I_{S}) atom were constructed. After the construction of $\text{Cd}_{1-x}\text{Mn}_x\text{S}$ ($x=6.25\%$) supercell with interstitial Cd or S atom, atom relaxation and optimization of crystal structure were carried out. Electron band structure, density of states were calculated, and total energy have been defined (Fig. 7,8). In the case of interstitial Cd atom, the band gap is equal to $E_g=1.35$ eV, total energy is equal to $E_T=-60817.73$ eV (Fig. 7). For the interstitial S atom, the band gap is equal to $E_g=1.75$ eV, and total energy is equal to $E_T=-59624.67$ eV (Fig. 8). Figures 7 and 8 show that interstitial Cd or S atoms in crystal structure lead to an increase in the band gap.

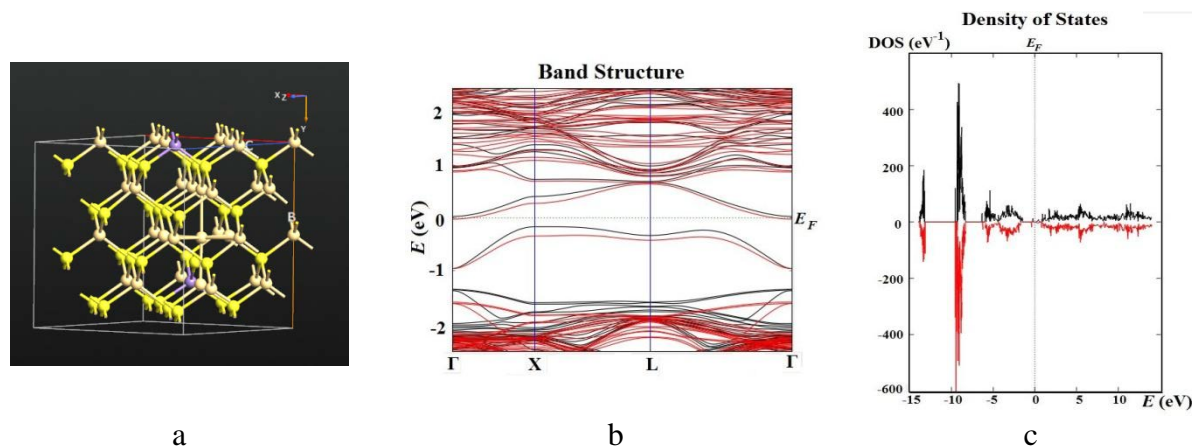


Fig. 9. Frenkel pair in $\text{Cd}_{1-x}\text{Mn}_x\text{S}$, $x = 0.625$; a – bulk configuration; b – EBS; c – DOS

Supercell of $\text{Cd}_{1-x}\text{Mn}_x\text{S}$ of 64 atoms with Frankel pair was constructed. After the construction of $\text{Cd}_{1-x}\text{Mn}_x\text{S}$ ($x=6.25\%$) supercell with Frankel pair, atom relaxation and optimization of crystal structure were carried out. Electron band structure, density of states were calculated, and total energy have been defined. In the case of Frankel pair, the band gap is equal to $E_g=2$ eV, total energy is equal to $E_t=-60817.77$ eV (Fig. 9).

It can be concluded that vacancy, interstitial atom, or Frenkel pair type defects in crystal lead to an increase in the band gap, Fermi level shifts towards the valence or conduction band (Table 2).

Table 2. Band gap and total energy for Interstitial Cd (S) atom and Cd (S) vacancy in $\text{Cd}_{1-x}\text{Mn}_x\text{S}$, $x=0.25$

$x=0.0625$	Ideal	V_{Cd}	V_S	I_{Cd}	I_S	FP
E_g , eV	1.25	1.55	1.3	1.35	1.75	2
E_t , eV	-59267.93	-57712.51	-58907.65	-60817.73	-59624.67	60817.77

3. Conclusion

Ab initio calculations have been performed to analyze the electronic band structure of an ideal and defective $\text{Cd}_{1-x}\text{Mn}_x\text{S}$ SMSC ($x = 0.25; 0.0625$). It has been defined that with an increase in Mn ion concentration in the $\text{Cd}_{1-x}\text{Mn}_x\text{S}$, there is an increase in the band gap and an increase in the total energy. The calculations show that the defects as a vacancy, interstitial atom, or Frenkel pair in a crystal lead to an increase in the band gap, shifting the Fermi level towards the valence or conduction band.

References

1. Munde BS, Ravangave LS. Physical and spectroscopic characterization of chemically deposited $\text{Cd}_{1-x}\text{Mn}_x\text{S}$ thin films. *IOSR Journal of Applied Physics*. 2017;9(3): 85-89.
2. Munde BS, Mahewar RB, Ravangave LS. Study of spectroscopic properties of $\text{Cd}_{0.6}\text{Mn}_{0.4}\text{S}$ chemical bath deposited thin film for solar cell applications. *International Journal of Research and Analytical Reviews*. 2018;5(3): 962-966.
3. Mali AE, Gaikwad AS, Borse SV, Ahire RR. Influence of Mn^{2+} magnetic ions on the properties of $\text{Cd}_{1-x}\text{Mn}_x\text{S}$ thin films synthesized by chemical bath deposition. *Journal of Nano- and Electronic Physics*. 2021;13(1): 01004.
4. Girish M, Sivakumar R, Sanjeeviraja C. Tuning the properties of $\text{Cd}_{1-x}\text{Mn}_x\text{S}$ films deposited by nebulized spray pyrolysis. *Optik - International Journal for Light and Electron Optics*. 2021;227(4): 166088.
5. Potapenko KO, Kurenkova AY, Bukhtiyarov AV, Gerasimov EY, Cherepanova SV, Kozlova EA. Comparative Study of the Photocatalytic Hydrogen Evolution over $\text{Cd}_{1-x}\text{Mn}_x\text{S}$ and $\text{CdS}-\beta\text{-Mn}_3\text{O}_4\text{-MnOOH}$ Photocatalysts under Visible Light. *Nanomaterials*. 2021;11(2): 355.
6. In-Hwan C, Peter YY. Structural and optical properties of cubic-CdS and hexagonal-CdS thin films grown by MOCVD on GaAs substrates using a single source precursor $\text{C}_{14}\text{H}_{30}\text{CdN}_2\text{S}_4$. *Physica Status Solidi (b)*. 2005;242: 1610-1616.
7. Basudev P, Ashwani KS, Asim KR. Conduction studies on chemical bath-deposited nanocrystalline CdS thin films. *Journal of Crystal Growth*. 2007;304(2): 388-392.

8. Feng W, Wee BT, Yong Z, Xianping F, Minquan W. Luminescent nanomaterials for biological labeling. *Nanotechnology*. 2006;17: R1-R13.
9. Wu XJ, Shen DZ, Zhang Z, Liu KW, Li BH, Zhang JY, Lu YM, Zhao DX, Yao B, Ren XG, Fan XW. Characterization of Cd_{1-x}FexS diluted magnetic semiconductors grown at near phase conversion temperature. *Solid State Communications*. 2007;141: 344-347.
10. Franciosi W, Niles DW, Reifenberger R, Quaresima C, Copozi M, Perfetti P. Electronic structure of Cd_{1-x}MnxS ternary semimagnetic alloys. *Physical Review B*. 1990;41: 5969-5978.
11. Badera N, Godbole B, Srivastava SB, Vishwakarma PN, Chandra LSSh. Jain D, Sathe VG, Ganesan V. Photoconductivity in Cd_{1-x}MnxS thin films prepared by spray pyrolysis technique. *Solar Energy Materials and Solar Cells*. 2008;92: 1646-1651.
12. Ahmed N, Nabi A, Nisar J, Tariq M, Javid MA, Nasim MH. First principle calculations of electronic and magnetic properties of Mn-doped CdS (zinc blende): a theoretical study. *Materials Science-Poland*. 2017;35(3): 479-485.
13. Masrour R, Hlil EK. Correlation of electronic structure and magnetic moment in Ga_{1-x}MnxN: First-principles, mean field and high temperature series expansions calculations. *Physica A*. 2016;456: 215-221.
14. Mounkachi O, Salmani E, El Moussaoui H, Masrour R, Hamedoun M, Ez-Zahraouy H, Hlil EK, Benyoussef A. High blocking temperature in SnO₂ based super-paramagnetic diluted magnetic semiconductor. *Journal of Alloys and Compounds*. 2014;614: 401-407.
15. Rkhioui A, Masrour R, Hlil EK, Benyoussef A, Hamedoun M, Bahmad L. Electronic and Magnetic Properties of Ga_{1-x}MxA (M = Mn and Cr; A = As and N): Ab Initio Study. *Journal of Superconductivity and Novel Magnetism*. 2015;28: 3419-3428.
16. Masrour R, Rkhioui A, Hlil EK, Hamedoun M, Benyoussef A, Bahmad L. Calculated Ab-Initio of Co-doped Zn_{1-x-y}AxB_yO (A=Mo; B=Mn, Cr). *Journal of Superconductivity and Novel Magnetism*. 2015;28: 125-129.
17. Rkhioui A, Masrour R, Hlil EK, Bahmad L, Hamedoun M, Benyoussef A. Study of Electronic and Magnetic Properties of Zn_{1-x}MxO (M = Mn and Cr) by ab initio Calculations. *Journal of Superconductivity and Novel Magnetism*. 2013;26: 3469-3474.
18. Kumar S, Kumar A, Ahluwalia PK. First principle study of manganese doped cadmium sulphide sheet. *AIP Conference Proceedings*. 2014;1591(1): 1732.
19. Rantala TT, Rantala TS, Lantto V, Vaara J. Surface relaxation of the (1010) face of wurtzite CdS. *Surface Science*. 1996;352-354: 77-82.
20. Nabi A. The electronic and the magnetic properties of Mn doped wurtzite CdS: First-principles calculations. *Computer Material Science A*. 2016;112: 210-218.
21. Mehrabova MA, Orujov HS, Hasanov NH, Kazimova AI, Abdullayeva A. Ab Initio Calculations of Defects in CdMnSe Semimagnetic Semiconductors. *Mechanics of Solids*. 2020;55(1): 108-113.
22. Mehrabova MA, Hasanov NH, Huseynov NI, Kazimova AI. Ab initio calculations of defects in Cd_{1-x}MnxTe(Se) semimagnetic semiconductors. *Journal of Radiation Researches*. 2020;7(2): 39-42.
23. Mehrabova MA, Orujov HS, Nuriyev HR, Hasanov NH, Abdullayeva AA, Suleymanov ZI. Ab-initio calculations of electronic structure of CdFeTe and optical properties. *Conference Proceedings Modern Trends In Physics*. 2019: 39-42.
24. Mehrabova MA, Hasanov NH, Huseynov NI, Kazimova AI, Asadov FG. Effect of defects on electronic structure of Cd_{1-x}MnxSe semimagnetic semiconductors. *Journal of Radiation Reserches*. 2018;5(2): 46-50.

25. Mehrabova MA, Nuriyev HR, Orujov HS, Nazarov AM, Sadigov RM, Poladova VN. Defect formation energy for charge states and electrophysical properties of CdMnTe. *Proc. SPIE Photonics, Devices and Systems VI, SPIE*. 2015;9450: 945001-9450010.
26. Srivastava P, Kumar P, Singh K. Room temperature ferromagnetism in magic-sized Cr-doped CdS diluted magnetic semiconducting quantum dots. *Journal of Nanoparticle Research*. 2011;13(10): 5077-5085.
27. Al-Jawad SMH. Optoelectronic characteristics and optical properties for Cd_{1-x}Mn_xS nanocrystalline thin films prepared by chemical bath deposition. *International Journal of Application or Innovation in Engineering & Management*. 2014;3(2): 329-333.

THE AUTHORS

Mehrabova M.A.

e-mail: mehrabova@mail.ru

ORCID: 0000-0003-4417-0522

Panahov N.T.

e-mail: panahovn@yahoo.com

ORCID: 0000-0002-9178-0641

Hasanov N.H.

e-mail: n.h.hasanov@rambler.ru

ORCID: 0000-0002-5122-4712